Unified Strength Model for FRP Confined Heat-damaged Circular and Square Concrete Columns

Javad Shayanfar [1], Hassan Jafarian Kafshgarkolaei [2], Joaquim A. O. Barros [3] and Mohammadali Rezazadeh [4]

[1] PhD Candidate, ISISE, Department of Civil Engineering, University of Minho, Azurém 4800-058 Guimarães, Portugal, arch3d.ir@gmail.com (corresponding author)

[2] Postdoc Researcher, ISISE, Department of Civil Engineering, University of Minho, Azurém 4800-058 Guimarães, Portugal, hasan.jafarian@gmail.com

[3] Full Prof., ISISE, IBS, Department of Civil Engineering, University of Minho, Azurém 4800-058 Guimarães, Portugal, barros@civil.uminho.pt

[4] Lecturer, Civil Eng., Department of Mechanical and Construction Engineering, Northumbria University, Newcastle upon Tyne, NE1 8ST, United Kingdom, mohammadali.rezazadeh@northumbria.ac.uk

Abstract

Although a variety of analytically modeling approaches have been developed to simulate axial response of Fiber-Reinforced Polymer (FRP) confined concrete columns, little effort has been dedicated to the development of simple but robust predictive models for heat-damaged concrete columns with FRP confinement. This study aims to present a new unified strength model for predicting the peak compressive strength of FRP confined heat-damaged concrete with circular/square cross-section columns, applicable to both ambient and elevated temperature conditions. In order to achieve the highest level of reliability and predictive performance, a large database of experimental results available in the literature was assembled. In this model, the influences of column size, sectional non-circularity, and pre-existing thermal-induced damage in terms of confinement-induced improvements were considered in the model establishment based on regression analysis. The reliability of the developed model is demonstrated by simulating experimental counterparts and also comparing it to the predictive performance of existing strength models.

Keywords: Heat-damaged concrete columns; Peak compressive strength; Unified model; FRP confinement;

1- Introduction

During fire exposure, depending on its intensity, the concrete characteristics are deteriorated due to the substantial changes in its chemical and physical properties (Kodur and Sultan [1], Raut and Kodur [2]). Accordingly, in case of fire occurrence, the serviceability, durability and ultimate seismic capacities of a concrete structure would be affected significantly, and depending on the fire-damaged intensity, safety requirements can recommend its demolishment (Demir *et al.* [3]). Due to high costs and detrimental environmental impact of demolishing and reconstruction alternatives, a post-fire retrofitting solution should be considered to reinstate the structural performance of fire-damaged concrete elements. The application of externally bonded fiber-reinforced-polymer (FRP) composites for confining the fire-damaged concrete columns have been established as a potentially promising and viable method (Bisby *et al.* [4] and Ouyang *et al.* [5]).

In the past three decades, numerous experimental, numerical and analytical research studies have been carried out to investigate the capability of FRP confining technique in enhancing axial and dilation behavior of concrete columns (at the ambient condition) subjected to axial compressive loadings [6-12]. For the case of FRP fully confined circular cross-section concrete columns (FFCC in Fig. 1a), Kaeseberg *et al.* [12] evidenced that the FRP confinement of concrete elements of medium strength class is more effective than of concrete elements of the high-strength class. Jamatia and Deb [13] experimentally assessed the effect of the cross-section diameter of FFCC specimens (known as size effect) on their axial and dilation responses. It was demonstrated that for large-sized specimens confined lightly by FRP jacket (insufficient confinement stiffness), the size effect phenomenon has a considerable reduction in terms of axial strength and deformability, compared to small-sized specimens with the same confinement stiffness, which was also verified by Thériault *et al.* [14] and Elsanadedy *et al.* [8]. Wang and Wu [7] verified that the increase in FRP fully confinement-induced

enhancements is more pronounced in FFCC than in concrete columns of square cross-section (FFSC in Fig. 1a), which is attributed to non-circularity effect (also known as shape effect). Shan *et al.* [9] showed that the magnitude of non-circularity effect on the effectiveness of FRP confinement system of FFSC is significantly dependent on the corner radius ratio ($R_b = 2r/b$ where b and r define the length of cross-section side and corner radius, respectively, Fig. 1a). It was demonstrated that by reducing R_b from one to zero (the column shape is transformed from FFCC to a FFSC with sharp edges), the capability of the confining system, in terms of axial strength and deformability, is noticeably reduced.

On the other hand, the application of FRP confinement technique to the case of heat-damaged concrete specimens, already submitted to a certain heating process scheme (as typically illustrated in Fig. 1b), has so far received little attention. Bisby *et al.* [4] examined experimentally the axial and dilation behavior of carbon FRP (CFRP) fully confined circular heat-damaged concrete columns (FFCC-H in Fig. 1c) exposed to different maximum exposure temperature levels (T_m in Fig. 1b) as 300, 500 and 686 °C. These authors verified that FRP confinement solution is a reliable technique for improving axial and dilation responses of FFCC-H. Furthermore, the strength ratio (defined as the ratio of peak axial strength of FFCC-H and FFCC) showed an almost downward trend with the increase of T_m, with values of 1.03, 0.92 and 0.87 for T_m equal to 300, 500 and 686 °C, respectively. However, the ratio of peak axial strength of FFCC-H and that of its corresponding unconfined one was 2.11, 2.26, 2.70 and 3.49 for the cases of T_m equal to 300, 500 and 686 °C, respectively, representing an increase in FRP confinement-induced enhancements with the increase of T_m. Lenwari *et al.* [15] tested FFCC-H specimens under axial loading to assess the influences of the heating scheme properties (i.e. exposure duration, cooling regime and T_m) and unconfined concrete compressive strength on the axial response of FFCC-H. It was shown that the cooling regime

of specimens (Fig. 1b) by air-cooled results in more axial strength compared to water-cooled. Moreover, the loss in terms of residual properties is more considerable for low-strength concrete specimens than high-strength ones. Ouyang *et al.* [5] tested FFCC-H specimens under axial loading to examine the effect of thermal-induced damage on their axial and dilation behavior. It was verified that the lateral expansion and axial stress-strain curve of FFCC-H depend strongly on the level of T_m. Besides, there was no obvious relation between FRP hoop strain measured at the rupture stage and T_m. Song *et al.* [16] experimentally demonstrated that FRP confinement system is a promising strengthening technique to improve axial and dilation behavior of FRP fully confined square heat-damaged concrete columns (FFSC-H, Fig. 1). It was also found that the effectiveness of FRP confining system is more pronounced in heat-damaged concrete exposed to high level of T_m than in concrete columns at ambient conditions.

A variety of axial strength models with a design framework (i.e. CNR DT 200/2004 [17], Wei and Wu [18], Nistico and Monti [19], ACI 440.2R- 17 [20] and *fib* [21]) has been suggested for the estimation of the peak compressive strength (f_{cu}) of FRP confined concrete columns under axial loading. Most of these models was developed and calibrated based on a test database of FFCC, in which a relation between f_{cu} and confinement pressure generated by FRP jacket is established based on a regression analysis technique. For the case of FFSC, the non-circularity effect, leading to a loss in the confinement-induced enhancement compared to FFCC, is generally simulated by using the following approaches: i) adopting the theoretical-based concept of confinement efficiency factor which simulates the horizontal arching action (i.e. Lam and Teng [22], Shayanfar *et al.* [23]); and ii) developing empirical formulations, as a main function of the corner radius ratio (R_b), based on a test database of FFSC (Wei and Wu [18] and Nistico and Monti [19]). For the case of FFCC-H, Bisby *et al.* [4] adapted ACI 440.2R-08 [24]'s model, which was developed exclusively for FFCC at ambient condition, to predict

f_{cu}. In this model, the effectiveness of FRP confinement on f_{cu} of heat-damaged concrete is assumed identical to its effect on that of concrete column with the same compressive strength at ambient conditions. Ouyang *et al.* [5] examined this approach by adopting the predictive models suggested by Lam and Teng [25], and Ozbakkaloglu and Lim [26] (exclusively developed for FFCC) for the estimation of experimental f_{cu} of FFCC-H. It was shown that this approach results in very conservative predictions of the experimental counterparts, which was also verified by Song *et al.* [16] for the case of FFSC-H. Accordingly, the applicability of existing axial strength models, which were developed/calibrated for FFCC or/and FFSC at ambient condition, is, at least, arguable for FFCC-H/FFSC-H. Hence, an axial strength model with design framework to predict f_{cu} of FFCC-H/FFSC-H at elevated temperature having a unified character with FFCC/FFSC at ambient condition is still lacking. On the other hand, most of the existing strength models were calibrated based on regression analysis performed on a test database of FFCC/FFSC with a short range of key variables i.e. concrete properties, confinement stiffness, FRP rupture strain, specimen dimension and corner radius ratio. Hence, by providing a more comprehensive database including wide-ranging variables, the recalibration of these strength models might improve their reliability and performance.

The present paper aims to introduce a new strength model for the prediction of peak compressive strength (f_{cu}) of FRP confined heat-damaged concrete with circular/square cross-section columns, applicable to ambient and elevated temperature conditions. For this purpose, a large test database including 1915 test specimens with 1517 FFCC, 254 FFSC, 109 FFCC-H, and 35 FFSC-H available in the literature was assembled. Based on FFCC specimens in the database, a new strength model is developed considering the size effect. Using this model, the influence of the non-circularity effect is reflected empirically in terms of confinement-induced enhancements of FFSC. For the case of FFCC-H/FFSC-H, the influence of pre-existing

thermal-induced damage in terms of confinement effectiveness is simulated through regression analysis based on a parametric study on confinement effectiveness and maximum exposure temperature levels (T_m). Finally, the verification of the proposed axial strength model and its comparative assessment with existing ones are revealed through predicting the f_{cu} of the experimental counterparts.

2- Test Database

This section introduces the geometry and material details of the test specimens along with their experimental peak axial strength assembled in the database. This database consists of 1915 test specimens that can be divided into three groups: A) fully FRP confined circular concrete columns at ambient condition (FFCC) with 1517 specimens; B) fully FRP confined square concrete columns at ambient condition (FFSC) with 254 specimens; C) fully FRP confined circular/square heat-damaged concrete columns at elevated temperature (FFCC-H/FFSC-H) with 144 specimens. The database does not include the specimens in the following conditions: i) having incomplete information of the geometry and material details; ii) with steel hoops/stirrups; iii) having a premature failure mode of FRP debonding; iv) with FRP partial/ hybrid/ helicoidal confinement arrangement; v) tested under eccentric axial loading condition; vi) with almost sharp corners (for the case of FFSC/FFSC-H) where $R_b = 2r/b \le 0.05$ or $r \le 0.025b$; vii) with a maximum exposure temperature (T_m) more than $800\ ^\circ\mathrm{C}$ (for the case of FFCC-H/FFSC-H); viii) with a peak axial compressive strength (f_{cu}) less than $1.05 f_{c0}$.

Table 1 and Fig. 2 include a summary of the collected test database of FFCC, FFSC, FFCC-H and FFSC-H with a wide range of key influential parameters.

As presented, the axial strength of unconfined concrete (f_{c0}) is in the range of 5.5-204 MPa with the mean value (MV) and Coefficient of Variation (CoV) of 43.2 MPa and 0.723,

144 respectively. The normalized peak axial strength of the confined specimens (f_{cu}/f_{c0}) varies
145 from 1.05 to 13.8 with MV and CoV of 2.17 and 0.562, respectively. The cross-section
146 dimension of the concrete specimens (b) is in the range of 50-400 mm with MV and CoV of
147 147 mm and 0.297, respectively. The specimen height (L) varies from 100 to 1200 mm with
148 MV and CoV of 313 mm and 0.370, respectively. The database includes concrete specimens
149 confined by different types of FRP material, as carbon (CFRP), aramid (AFRP), basalt (BFRP),
150 glass (GFRP), polyethylene terephthalate (PET) and polyethylene naphthalate (PEN) fibers.
151 The FRP elastic modulus (E_f) varies from 9.5 to 657 GPa with MV and CoV as 174 GPa and
152 0.589, respectively. The ultimate tensile strain of FRP sheets (ε_{fu}) is in the range of 0.004-
153 0.10 with MV and CoV of 0.024 and 0.782, respectively. For the case of square cross-section
154 column specimens (FFSC), the corner radius ratio (R_b) varies from 0.07 to 0.80 with MV and
155 CoV of 0.36 and 0.527, respectively. Regarding the FRP confined heat-damaged concrete
156 column specimens (FFCC-H/FFSC-H), the maximum exposure temperature (T_m) is in the
157 range of 200-800 °C with MV and CoV of 525 °C and 0.369, respectively. Among 144 heat-
158 damaged specimens, 109 specimens have circular cross-section (FFCC-H) and the remaining
159 35 specimens represent FFSC-H with square cross-section. Furthermore, in heat-damaged
160 specimens, the cooling regime of 115 and 29 specimens was in air and water, respectively.

161 Studies conducted by [1,2, 27-29] Kodur and Sultan (2003), Hertz (2005), and Raut and Kodur
162 (2011) demonstrated that the axial compressive strength of unconfined heat-damaged concrete
163 columns is strongly dependent on the level of the maximum exposure temperature (T_m). In the
164 present study, based on a preliminarily assessment on the existing models (i.e. [27-30]), the
165 model presented by Chang *et al.* [28] was adopted for the determination of the deteriorated
166 compressive strength of unconfined heat-damaged concrete columns (f_{c0}^{T}), which can be
167 calculated by:

$$f_{c0}^{T} = \left(1.01 - 0.00055T_m\right) f_{c0} \qquad \text{for } T_m \le 200\ ^\circ\text{C} \tag{1a}$$

$$f_{c0}^{T} = \left(1.15 - 0.00125T_m\right) f_{c0} \qquad \text{for } T_m \ge 200\ ^\circ\text{C} \tag{1b}$$

where f_{c0}^{T} becomes equal to zero for the concrete column submitted to $T_m \ge 920\ ^\circ\text{C}$.

3- Existing Models

The models proposed by CNR DT 200/2004 [17], Wei and Wu [18], Nistico and Monti [19], ACI 440.2R- 17 [20] and *fib* [21] for the estimation of the peak axial strength of FRP fully confined concrete columns (f_{cu}), with a unified character for both cases of circular and square cross-sections, are presented in Table 2. In the models recommended by CNR DT 200/2004 [17], ACI 440.2R- 17 [20] and *fib* [21], the normalized peak axial strength (f_{cu}/f_{c0}) of FFCC/FFSC is expressed as a main function of normalized FRP confinement pressure ($f_{l,rup}/f_{c0}$) corresponding to FRP rupture ($\varepsilon_{h,rup}$) as (see Table 2):

$$\frac{f_{cu}}{f_{c0}} = 1 + \Delta_c = 1 + \alpha_1 \left(\frac{f_{l,rup}}{f_{c0}} \right)^{\alpha_2} \tag{2}$$

where Δ_c defines the FRP confinement-induced improvement; α_1 and α_2 are the calibration factors that are obtained based on a regression analysis performed with the experimental database of FFCC/FFSC. Furthermore, for FFSC, for the sake of cross-section unification, the concept of confinement efficiency factor (k_h), originally developed by Mander *et al.* [31], is adopted to consider the effect of non-circularity (also known as shape effect) induced by arching action phenomenon. On the other hand, in Wei and Wu [18] and Nistico and Monti [18], as presented in Table 2, f_{cu}/f_{c0} is determined based on the normalized ultimate confinement pressure ($f_{l,u}/f_{c0}$) corresponding to the ultimate tensile strain of FRP sheet (ε_{fu}) as:

$$\frac{f_{cu}}{f_{c0}} = 1 + \Delta_c = 1 + \alpha_3 \alpha_r \left(\frac{f_{l,u}}{f_{c0}} \right)^{\alpha_4} \quad (3)$$

where α_3 and α_4 are the calibration factors that are obtained based on a regression analysis performed with the experimental results of the database for the FFCC; α_r is the calibration factor determined by applying the model developed for FFCC to the test specimens of FFSC, to empirically formulate the effect of non-circularity as a function of corner radius ratio ($R_b = 2r/b$). In this study, it is also investigated the reliability of these axial strength models, which were developed/calibrated based on the tested concrete specimens at ambient conditions (FFCC/FFSC), for predicting the peak strength of heat-damaged concrete columns (FFCC-H/FFSC-H). Note that to calculate f_{cu} of FFCC-H/FFSC-H, f_{c0}^{T} (Eq. (1)) can be used in Eq. (2) and (3) instead of f_{c0} based on the existing assumption recommended by Bisby *et al.* [4] for the substitution of the mechanical properties of unconfined heat-damaged concrete with those of unconfined concrete one at ambient condition.

4- Proposed Model

In this section, a new model is proposed for the determination of peak axial strength of plain concrete and heat-damaged concrete columns (f_{cu}) confined by FRP jacket based on regression analyses on the assembled database (Table 1). The procedure to establish the unified model is briefly presented as follows:

i) Development of an axial strength model developed exclusively for the case of FFCC based on regression analysis technique to calibrate its model parameters, using 1517 test specimens of FFCC.

ii) Extension of the strength model, developed for FFCC, for the case of FFSC by considering the influence of non-circularity effect on FRP confinement-induced improvements, using 254 test specimens of FFSC for the calibration.

iii) Extension of the strength model developed for FFCC/FFSC for the case of FFCC-H/FFSC-H, by taking into account the influence of pre-existing thermal damage on FRP confinement-induced improvements, using 144 test specimens of FFCC-H/FFSC-H for the calibration.

In the present study, based on CNR DT 200/2004 [17]'s recommendation, FRP confinement pressure ($f_{l,rup}$) is calculated as

$$f_{l,rup} = 2\frac{n_f t_f E_f}{b}\varepsilon_{h,rup} = 2K_L\varepsilon_{h,rup} \tag{4}$$

in which

$$K_L = \frac{n_f t_f E_f}{b} \qquad (E_f \text{ in MPa, and } t_f \text{ and } b \text{ in mm}) \tag{5}$$

where n_f is the number of FRP layers; t_f is the nominal thickness of an FRP layer; E_f is the modulus of elasticity of FRP; b is the cross-section dimension.

4.1- FFCC at ambient conditions

For the case of FFCC, the normalized peak axial strength (f_{cu}/f_{c0}) is in general expressed as a main function of normalized FRP confinement pressure ($f_{l,rup}/f_{c0}$) corresponding to FRP rupture strain ($\varepsilon_{h,rup}$). Accordingly, f_{cu}/f_{c0} can be written based on Eqs. (2) and (4) as:

$$\frac{f_{cu}}{f_{c0}} = 1+\Delta_c = 1+k_0\left(\frac{f_{l,rup}}{f_{c0}}\right)^{k_1} = 1+k_0\left(2\right)^{k_1}\left(\frac{K_L}{f_{c0}}\varepsilon_{h,rup}\right)^{k_1} \tag{6}$$

where Δ_c defines the FRP confinement-induced improvement, and k_0 and k_1 are the calibration factors. By assuming $\varepsilon_{h,rup}$ is directly proportional to FRP ultimate tensile strain (ε_{fu}) as $\varepsilon_{h,rup} = \alpha_{\varepsilon h}\varepsilon_{fu}$ where $\alpha_{\varepsilon h}$ is a constant coefficient (Lam and Teng [25]), Eq. (6) can be rearranged as:

$$\frac{f_{cu}}{f_{c0}} = 1 + k_0 \left(2\alpha_{\varepsilon h}\right)^{k_1} \left(\frac{K_L}{f_{c0}}\varepsilon_{fu}\right)^{k_1} \tag{7}$$

In order to develop a regression-based predictive model, Eq. (7) was restructured as follows:

$$\frac{f_{cu}}{f_{c0}} \simeq 1 + k_2 \left(K_L\right)^{k_3} \left(f_{c0}\right)^{k_4} \left(\varepsilon_{fu}\right)^{k_5} \qquad (f_{c0} \text{ in MPa}) \tag{8}$$

where k_2, k_3, k_4 and k_5 are the calibration factors. Through a regression analysis performed on 1517 test specimens of FFCC, these calibration factors were determined as $k_2 = 4$, $k_3 = 0.8$, $k_4 = -1.2$ and $k_5 = 0.65$. Predictive performance of Eq. (8) is demonstrated in Fig. 3, where f_{cu}^{Exp} and f_{cu}^{Ana} are the peak axial strength registered experimentally and obtained with Eq. (8). As shown, there is a good agreement between experimental and analytical results based on the obtained statistical indicators of *Mean Value* (MV) = 1.004, *Coefficient of Variation* (CoV) = 0.223, *Mean Absolute Percentage Error* (MAPE) = 0.161, *Mean Squared Error* (MSE) = 0.320 and *R-squared* (R^2) = 0.821.

On the other hand, by defining Y_1 as the ratio of confinement-induced improvements obtained analytically over experimentally ($Y_1 = \left(\Delta_c\right)^{Ana} / \left(\Delta_c\right)^{Exp}$, where $\left(\Delta_c\right)^{Ana}$ was determined based on Eq. (8), this error index can be expressed as:

$$Y_1 = \frac{(\Delta_c)^{Ana}}{(\Delta_c)^{Exp}} = \frac{\left(\frac{f_{cu}}{f_{c0}}\right)^{Ana} - 1}{\left(\frac{f_{cu}}{f_{c0}}\right)^{Exp} - 1} = \frac{k_2 (K_L)^{k_3} (f_{c0})^{k_4} (\varepsilon_{fu})^{k_5}}{\left(\frac{f_{cu}}{f_{c0}}\right)^{Exp} - 1} \quad (9)$$

237 In order to evaluate the influence of column dimension size ($b/150$) on the effectiveness of
238 FRP confinement system in terms of the peak strength of FFCC, the relation of Y_1 and $b/150$
239 is analysed in Fig. 4a. As can be seen, there is an upward trend for Y_1 by increasing $b/150$,
240 representing that Eq. (8) leads to underestimation for small-sized specimens, and
241 overestimation for the case of large-sized ones, attributed to the size effect. Based on regression
242 analysis performed on FFCC, the best-fit relation of Y_1 and $b/150$ was resulted in:

$$Y_1 = k_6 \left(\frac{b}{150}\right)^{k_7} = 1.07 \left(\frac{b}{150}\right)^{0.3} \quad (10)$$

243 where the calibration factors of k_6 and k_7 were obtained as 1.07 and 0.3, respectively.
244 Therefore, based on Eqs. (8) and (10), f_{cu} of FFCC can be calculated by considering the size
245 effect as:

$$\frac{f_{cu}}{f_{c0}} = 1 + \frac{k_2}{Y_1} (K_L)^{k_3} (f_{c0})^{k_4} (\varepsilon_{fu})^{k_5} = 1 + 3.75 (K_L)^{0.8} (f_{c0})^{-1.2} (\varepsilon_{fu})^{0.65} \left(\frac{b}{150}\right)^{-0.3} \quad (11)$$

246 As shown in Fig. 4b, there is a suitable agreement between the predictions obtained from the
247 proposed Eq. (11) and those reported for the experimental counterparts. Furthermore, based on
248 the statistical assessment of the large experimental results, Eq. (11) revealed a better predictive
249 performance compared to Eq. (8), confirming the reliability of the size effect consideration.

250

251

252 **4.2- FFSC at ambient conditions**

253 On the other hand, by defining Y_2 as the ratio of confinement-induced improvements obtained
254 analytically over experimentally ($Y_2 = (\Delta_c)^{Ana} / (\Delta_c)^{Exp}$, where $(\Delta_c)^{Ana}$ was determined based
255 on Eq. (11), it can be written as:

$$Y_2 = \frac{(\Delta_c)^{Ana}}{(\Delta_c)^{Exp}} = \frac{\left(\frac{f_{cu}}{f_{c0}}\right)^{Ana} - 1}{\left(\frac{f_{cu}}{f_{c0}}\right)^{Exp} - 1} = \frac{3.75(K_L)^{0.8}(f_{c0})^{-1.2}(\varepsilon_{h,rup})^{0.65}\left(\frac{b}{150}\right)^{-0.3}}{\left(\frac{f_{cu}}{f_{c0}}\right)^{Exp} - 1} \quad (12)$$

256 In order to evaluate the non-circularity effect (R_b) on the peak strength of FFSC, the relation
257 of Y_2 and R_b was analysed in Fig. 5a. As can be seen, Eq. (11) did not exhibit appropriate
258 agreement when applied to square cross-section specimens. By decreasing R_b, Eq. (11)
259 resulted in remarkable overestimations in terms of the peak strength of the FFSC, particularly
260 square cross-section with almost sharp edges, which is attributed to the non-circularity effect.
261 Based on regression analysis performed on 254 test specimens of FFSC, the best-fit relation of
262 Y_2 and R_b resulted in:

$$Y_2 = k_8 (R_b)^{k_9} = 0.69 (R_b)^{-0.9} \geq 1 \quad (13)$$

263 where the calibration factors of k_8 and k_9 were determined as 0.69 and -0.9, respectively.
264 Accordingly, based on Eqs. (11) and (13), f_{cu} of FFSC can be calculated by considering the
265 non-circularity effect as:

$$\frac{f_{cu}}{f_{c0}} \simeq 1 + 3.75 k_r (K_L)^{0.8} (f_{c0})^{-1.2} (\varepsilon_{h,rup})^{0.65} \left(\frac{b}{150}\right)^{-0.3} \quad (14)$$

266 in which

$$k_r = \frac{1}{Y_2} = 1.45\left(R_b\right)^{0.9} \le 1 \tag{15}$$

As shown in Fig. 5b, there is a suitable agreement between the predictions obtained from the proposed Eq. (14) and those reported for the experimental counterparts of FFSC, based on the obtained statistical indicators.

4.3- FFCC-H and FFSC-H at elevated temperatures

In this section, the peak axial strength of FFCC-H and FFSC-H is determined by simulating the effect of pre-existing thermal damage on the effectiveness of FRP confinement system. By ignoring the effect of pre-existing thermal damage on the effectiveness of FRP confinement system, the peak axial strength of FFCC-H and FFSC-H can be determined from Eq. (14) by substituting f_{c0} with f_{c0}^{T} as:

$$\frac{f_{cu}}{f_{c0}^{T}} = 1 + \Delta_c \simeq 1 + 3.75k_r\left(K_L\right)^{0.8}\left(f_{c0}^{T}\right)^{-1.2}\left(\varepsilon_{h,rup}\right)^{0.65}\left(\frac{b}{150}\right)^{-0.3} \tag{16}$$

By defining Y_3 as the ratio of confinement-induced improvements obtained analytically over experimentally ($Y_3 = \left(\Delta_c\right)^{Ana} / \left(\Delta_c\right)^{Exp}$ where $\left(\Delta_c\right)^{Ana}$ was determined based on Eq. (16), it is obtained:

$$Y_3 = \frac{\left(\Delta_c\right)^{Ana}}{\left(\Delta_c\right)^{Exp}} = \frac{\left(\frac{f_{cu}}{f_{c0}^{T}}\right)^{Ana} - 1}{\left(\frac{f_{cu}}{f_{c0}^{T}}\right)^{Exp} - 1} = \frac{3.75k_r\left(K_L\right)^{0.8}\left(f_{c0}^{T}\right)^{-1.2}\left(\varepsilon_{h,rup}\right)^{0.65}\left(\frac{b}{150}\right)^{-0.3}}{\left(\frac{f_{cu}}{f_{c0}^{T}}\right)^{Exp} - 1} \tag{17}$$

Fig. 6a presents Y_3 *vs* $T_m/1000$ relationship obtained based on 144 test specimens of FRP heat-damaged concrete columns (FFCC-H/FFSC-H). As can be observed, by increasing the maximum exposure temperature (T_m) imposed to concrete, Eq. (16) leads to considerable

underestimation in terms of f_{cu}, depending on the level of T_m. It reveals that even though the axial strength of unconfined heat-damaged concrete (f_{c0}^{T}) was used in the determination of f_{cu}, the necessity of using an extra factor reflecting the effect of T_m in the confinement-induced improvements of FRP heat-damaged concrete columns is quite fundamental. As shown in Fig. 6a, the best-fit expression, as a function of T_m, was achieved as $Y_3 = 0.575\left(T_m/1000\right)^{-0.15} \le 1$, obtained from the regression analysis on 144 test specimens. However, the developed Y_3 was improved to the calibration factor of k_T, to consider the effects of cooling regime (in air or in water), concrete compressive strength (f_{c0}) and non-circularity (R_b), being determined from:

$$k_T = 3.5 k_{cm} k_{T0} \left(\frac{1.2 - 0.3R_b}{\sqrt{f_{c0}}} \right) \left(\frac{T_m}{1000} \right)^{-0.15} \le 1 \tag{18}$$

in which

$$k_{T0} = 2 - 4.5\left(\frac{T_m}{1000} \right) \le 1 \tag{19}$$

and $k_{cm} = 1.175$ for water-cooling method and $k_{cm} = 1$ for air-cooling method, based on the experimental results conducted by Lenwari *et al.* [15]. As a result, the developed model to predict the peak axial strength of FRP confined heat-damaged concrete columns at elevated conditions, having a unified character with that at ambient conditions, can be determined from:

$$\frac{f_{cu}}{f_{c0}^{T}} = 1 + 3.75 \frac{k_r}{k_T} \left(K_L\right)^{0.8} \left(f_{c0}^{T}\right)^{-1.2} \left(\varepsilon_{h,rup}\right)^{0.65} \left(\frac{b}{150} \right)^{-0.3} \tag{20}$$

The predictive performance of Eq. (20) in estimating f_{cu} registered experimentally is demonstrated in Fig. 6b. The achieved assessment indicators demonstrate that the developed equation was capable of accurately and uniformly predicting the experimental counterparts.

4-4- Model application

In this section, the predictive performance of proposed model is evaluated with respect to the various levels of the key model parameters. Fig. 7a demonstrates the relation of $f_{cu}^{Ana}/f_{cu}^{Exp}$ as error prediction with respect to K_L/f_{c0} representing a normalized confinement stiffness index. As shown, the predictions are in the interval of $[0.5-2.2]$ with almost uniform predictive performance for the considered range of K_L/f_{c0} values.

In Fig. 7b, the error distribution of $f_{cu}^{Ana}/f_{cu}^{Exp}$ is evaluated with concerning to the column dimension size ($b/150$). It was evidenced that the proposed model is able to provide uniform predictive performance for the considered range of $b/150$ values (Note that the larger dispersion for $b/150=1$ is due to its largest frequency in the complied database). Furthermore, it also confirms the reliability of the considered size effect term ($(b/150)^{-0.3}$) in the establishment of Eqs. (11 and 20).

Fig. 7c presents the model assessment for the case of square cross-section columns (FFSC/FFSC-H). As can be seen, there is a suitable agreement between analytical and experimental data with an error distribution in the interval of $[0.6-1.4]$ with almost a uniform predictive performance for $R_b<1$ (Note that the larger dispersion for $R_b=1$ is due to its largest frequency in the complied database). It also reveals the reliability of k_r in the development of the proposed model for FFSC/FFSC-H, which reflects the non-circularity effect.

In Fig. 7d, the model capability to estimate f_{cu}^{Ana} of FFCC-H/FFSC-H is demonstrated. As evidenced, the error distribution was achieved uniform with respect to maximum exposure temperature ($T_m/1000$) in the interval of $[0.8-1.25]$ (Note that the larger dispersion for environmental temperature is due to its largest frequency in the complied database). It can

confirm the reliability of the term of k_T in the establishment of the Eq. (20), in which the substantial influence of pre-existing thermal damage was reflected.

5- Comparative assessment

By performing a statistical assessment, Tables 3-5 compare the performance of existing and proposed models on predicting the f_{cu} registered experimentally on 1528, 323 and 144 tests with FFCC, FFSC and FFCC-H/FFSC-H, respectively, and collected in the database (Table 1).

For the case of FFCC, the results in Table 3 evidence that, although *fib* [21] and ACI 440.2R-17 [20] led to the best performance among the existing axial strength models, the developed model revealed better predictive performance in the estimation of the experimental counterparts.

For FRP fully confined square cross section concrete column (FFSC), the predictive performance of existing and developed axial strength models in the prediction of the experimental counterparts (f_{cu}^{Exp}) is presented in Table 4. As evidenced, among the existing models, Wei and Wu [18]'s model presented the best predictive performance based on the obtained statistical indicators. Even though the Wei and Wu [18] and developed models resulted in almost the same R^2, the developed model showed better performance.

For FRP fully confined circular/square heat-damaged concrete columns (FFCC-H/FFSC-H), Table 5 evidences that existing strength models led to a significant underestimation, even though the mechanical properties of unconfined heat-damaged concrete (f_{c0}^{T}) was adopted in the calculation of experimental f_{cu}. However, by reflecting the effect of pre-existing thermal damage in terms of FRP confinement-induced improvements of FFCC-H/FFSC-H through k_T factor in Eq. (20), the proposed model demonstrated a suitable agreement with the experimental results.

For the all cases covered in the test database (FFCC/FFSC/FFCC-H/FFSC-H), as shown in Table 6, the developed axial strength model (Eq. (20)) is the most reliable one compared to the other existing models based on the obtained statistical indicators.

6- Summary and conclusions

In this study, a new strength model was developed to predict peak compressive strength (f_{cu}) of heat-damaged concrete with circular/square cross-section columns concrete columns (FFCC-H/FFSC-H) with unified character for ambient condition cases (FFCC/FFSC). First, a new strength model was developed for the case of FFCC columns based on 1517 experimental results collected in the test database, in which the influence of the column size in confinement effectiveness was considered. Then, by applying this model on 254 test specimens of FFSC, the non-circularity effect was reflected empirically in terms of confinement-induced enhancements as a function of the corner radius ratio (R_b). Likewise, for the case of FFCC-H/FFSC-H, the detrimental influence of pre-existing thermal-induced damage was simulated as the main function of maximum exposure temperature levels (T_m) through regression analysis. The developed model has revealed a suitable reliability and also the best predictive performance compared to existing model, based on statistical indicators: MV = 0.987, CoV = 0.203, MAPE = 0.148, MSE = 0.259, R^2 = 0.854.

Since the limitation of the developed regression-based predictive model is rationally dependent on the range of input variables covered by the complied test database, it can be recalibrated and improved when a more comprehensive database supporting various ranges of the variables is available, resulting in an enhancement of the model reliability.

Data Availability Statement

All data and models related to the present study could be available from the corresponding author upon rational request.

Acknowledgments

This study is a part of the project ‘‘StreColesf-Innovative technique using effectively composite materials for the strengthening of rectangular cross-section reinforced concrete columns exposed to seismic loadings and fire’’, with the reference POCI-01-0145-FEDER-029485. The firs author also acknowledges the support provided by FCT PhD individual fellowship 2019 with the reference of “SFRH/BD/148002/2019”.

References

[1] Kodur, V. K. R., & Sultan, M. A. (2003). Effect of temperature on thermal properties of high-strength concrete. Journal of materials in civil engineering, 15(2), 101-107.

[2] Raut, N. K., & Kodur, V. K. R. (2011). Response of high-strength concrete columns under design fire exposure. Journal of Structural Engineering, 137(1), 69-79.

[3] Demir, U., Green, M. F., & Ilki, A. (2020). Post-fire seismic performance of reinforced precast concrete columns. PCI Journal, 65(6).

[4] Bisby, L. A., Chen, J. F., Li, S. Q., Stratford, T. J., Cueva, N., & Crossling, K. (2011). Strengthening fire-damaged concrete by confinement with fibre-reinforced polymer wraps. Engineering Structures, 33(12), 3381-3391.

[5] Ouyang, L. J., Chai, M. X., Song, J., Hu, L. L., & Gao, W. Y. (2021). Repair of thermally damaged concrete cylinders with basalt fiber-reinforced polymer jackets. Journal of Building Engineering, 44, 102673.

[6] Barros, J. A., & Ferreira, D. R. (2008). Assessing the efficiency of CFRP discrete confinement systems for concrete cylinders. Journal of Composites for Construction, 12(2), 134-148.

[7] Wang, L. M., & Wu, Y. F. (2008). Effect of corner radius on the performance of CFRP-confined square concrete columns: Test. Engineering structures, 30(2), 493-505.

[8] Elsanadedy, H. M., Al-Salloum, Y. A., Alsayed, S. H., & Iqbal, R. A. (2012). Experimental and numerical investigation of size effects in FRP-wrapped concrete columns. Construction and Building Materials, 29, 56-72.

[9] Shan, B., Gui, F. C., Monti, G., & Xiao, Y. (2019). Effectiveness of CFRP confinement and compressive strength of square concrete columns. Journal of Composites for Construction, 23(6), 04019043.

[10] Shayanfar, J., Rezazadeh, M., & Barros, J. A. (2020). Analytical model to predict dilation behavior of FRP confined circular concrete columns subjected to axial compressive loading. Journal of Composites for Construction, 24(6), 04020071.

[11] Shayanfar, J., Barros, J. A., & Rezazadeh, M. (2021). Generalized Analysis-oriented model of FRP confined concrete circular columns. Composite Structures, 270, 114026.

[12] Kaeseberg, S., Messerer, D., & Holschemacher, K. (2020). Experimental study on concrete under combined FRP–Steel confinement. Materials, 13(20), 4467.

[13] Jamatia, R., & Deb, A. (2017). Size effect in FRP-confined concrete under axial compression. Journal of Composites for Construction, 21(6), 04017045.

[14] Thériault, M., Neale, K. W., & Claude, S. (2004). Fiber-reinforced polymer-confined circular concrete columns: Investigation of size and slenderness effects. Journal of composites for construction, 8(4), 323-331.

[15] Lenwari, A., Rungamornrat, J., & Woonprasert, S. (2016). Axial compression behavior of fire damaged concrete cylinders confined with CFRP sheets. Journal of Composites for Construction, 20(5), 04016027.

[16] Song, J., Gao, W. Y., Ouyang, L. J., Zeng, J. J., Yang, J., & Liu, W. D. (2021). Compressive behavior of heat-damaged square concrete prisms confined with basalt fiber-reinforced polymer jackets. Engineering Structures, 242, 112504.

[17] CNR-DT 200. Guide for the design and construction of externally bonded FRP systems for strengthening existing structures. Italian National Research Council 2004.

[18] Wei, Y. Y., & Wu, Y. F. (2012). Unified stress–strain model of concrete for FRP-confined columns. Construction and Building Materials, 26(1), 381-392.

[19] Nisticò, N., & Monti, G. (2013). RC square sections confined by FRP: Analytical prediction of peak strength. Composites Part B: Engineering, 45(1), 127-137.

[20] ACI 440.2R-17. Guide for the design and construction of externally bonded FRP systems for strengthening concrete structures. American Concrete Institute (ACI): Farmington Hills MI USA 2017.

[21] Fib Bulletin 90. Externally applied FRP reinforcement for concrete structures. Task Group 5.1, International Federation for Structural Concrete 2019.

[22] Lam, L., & Teng, J. G. (2003). Design-oriented stress-strain model for FRP-confined concrete in rectangular columns. Journal of reinforced plastics and composites, 22(13), 1149-1186.

[23] Shayanfar, J., Barros, J. A., & Rezazadeh, M. (2022). Unified model for fully and partially FRP confined circular and square concrete columns subjected to axial compression. Engineering Structures, 251, 113355.

[24] ACI 440.2R-08. Guide for the design and construction of externally bonded frp systems for strengthening concrete structures. American Concrete Institute (ACI): Farmington Hills MI USA 2008.

[25] Lam, L., & Teng, J. G. (2003). Design-oriented stress–strain model for FRP-confined concrete. Construction and building materials, 17(6-7), 471-489.

[26] Ozbakkaloglu, T., & Lim, J. C. (2013). Axial compressive behavior of FRP-confined concrete: Experimental test database and a new design-oriented model. Composites Part B: Engineering, 55, 607-634.

[27] Hertz, K. D. (2005). Concrete strength for fire safety design. Magazine of concrete research, 57(8), 445-453.

[28] Chang, Y.F., Chen, Y.H., Sheu, M.S., and Yao, G.C. (2006). "Residual stress–strain relationship for concrete after exposure to high temperatures." Cement and Concrete Research, 36, 1999–2005.

[29] Li, L. Y., & Purkiss, J. (2005). Stress–strain constitutive equations of concrete material at elevated temperatures. Fire Safety Journal, 40(7), 669-686.

[30] Han, L. H., & Huo, J. S. (2003). Concrete-filled hollow structural steel columns after exposure to ISO-834 fire standard. Journal of Structural Engineering, 129(1), 68-78.

[31] Mander, J. B., Priestley, M. J., & Park, R. (1988). Theoretical stress-strain model for confined concrete. Journal of structural engineering, 114(8), 1804-1826.

List of Figures

List of Tables

Fig. 1

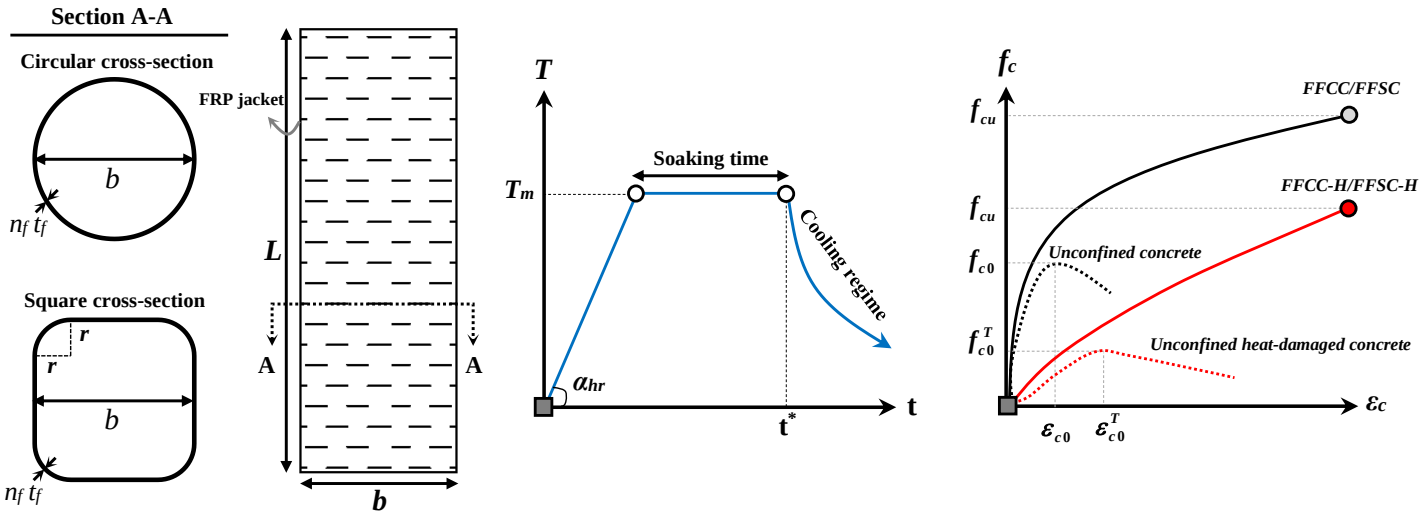

a) **b)** **c)**

Fig. 1. a) Details of FRP confined undamaged/heat-damaged concrete columns with circular/square cross-section (CC, SC); b) Typical exposure temperature (T) vs time (t) relation (heating and cooling processes); c) Typical axial stress-strain (f_c vs ε_c) curves

Note: T_m = maximum exposure temperature; α_{hr} = initial rate of heating process; t^* = exposure duration; f_{c0} = peak strength of unconfined concrete columns; f_{c0}^T = peak strength of unconfined heat-damaged concrete columns; f_{cu} = peak axial compressive strength of FRP confined specimens; ε_{c0} = axial strain at the peak stage; ε_{c0}^T = axial strain at the peak stage of heat-damaged concrete columns; L = height of the column; b = length of section dimension; r = length of corner radius; n_f = FRP layer number; t_f = nominal thickness of a FRP sheet.

Fig. 2

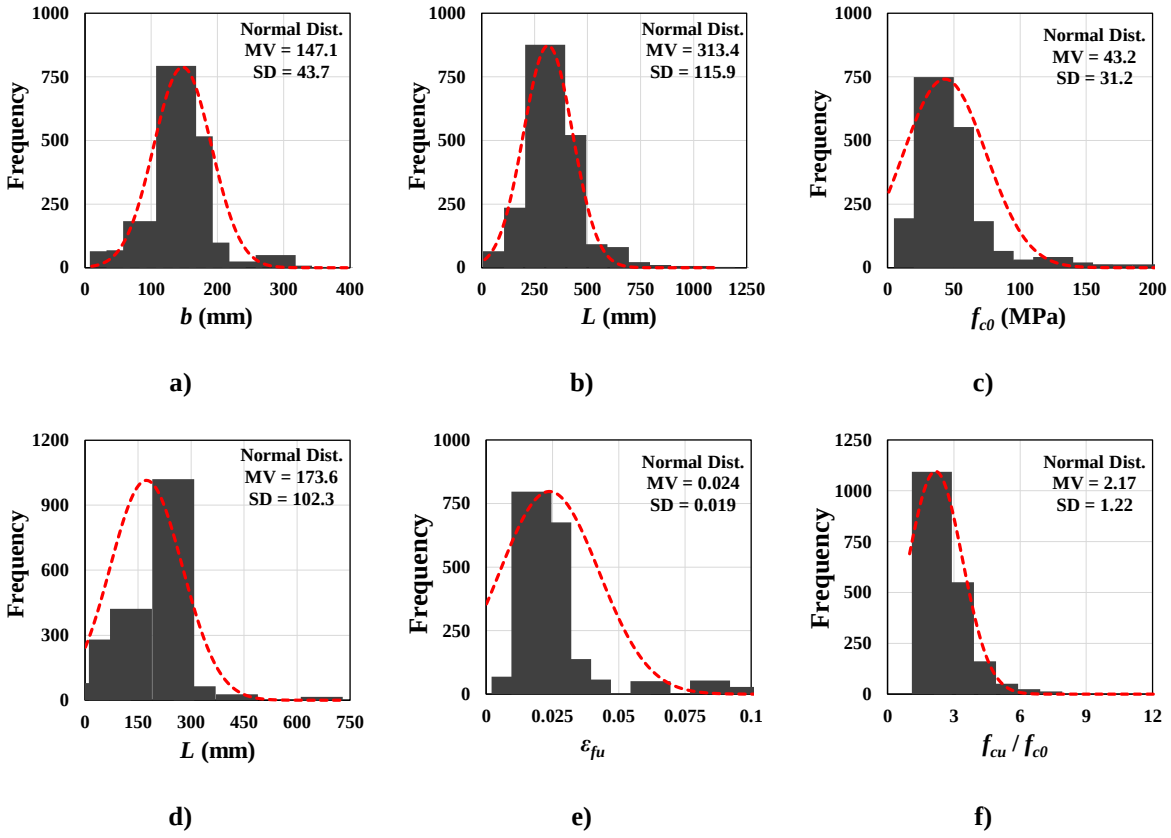

Fig. 2. Histogram demonstrating the variation of the key variables in the collected test database

Fig. 3

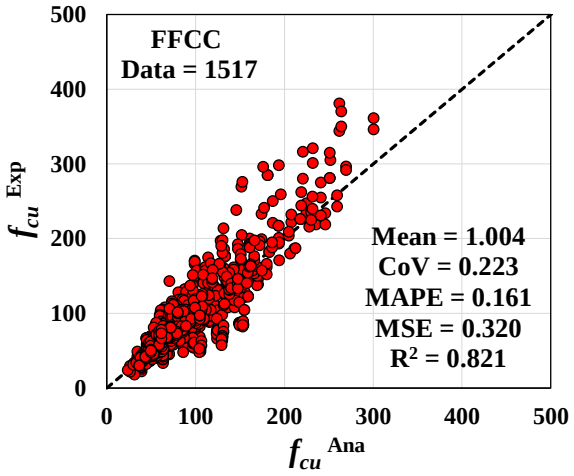

Fig. 3. Predictive performance of Eq. (8)

Fig. 4

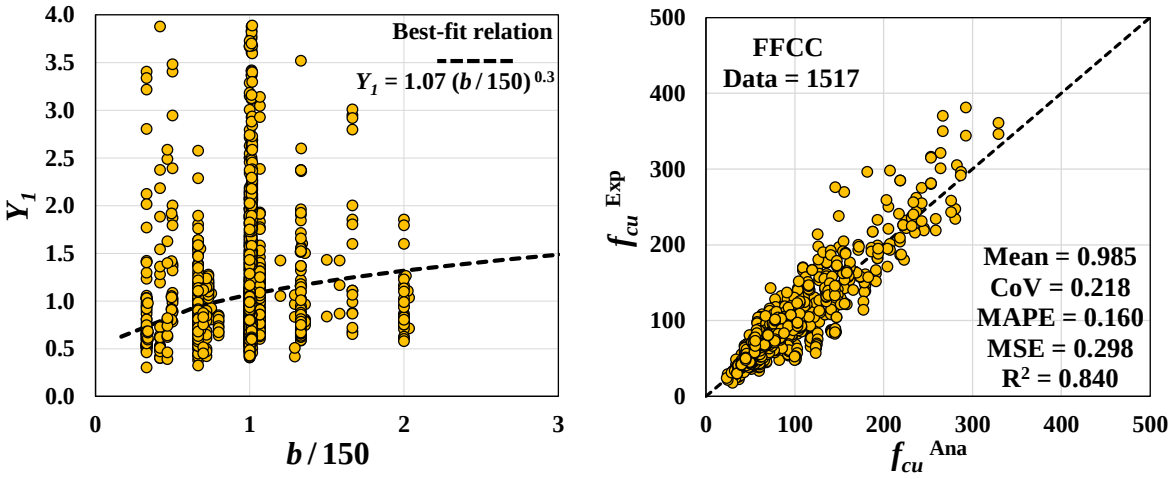

a) b)

Fig. 4. a) Relation of Y_1 versus b / 150; b) Model performance of Eq. (11) with the consideration of size effect

Fig. 5

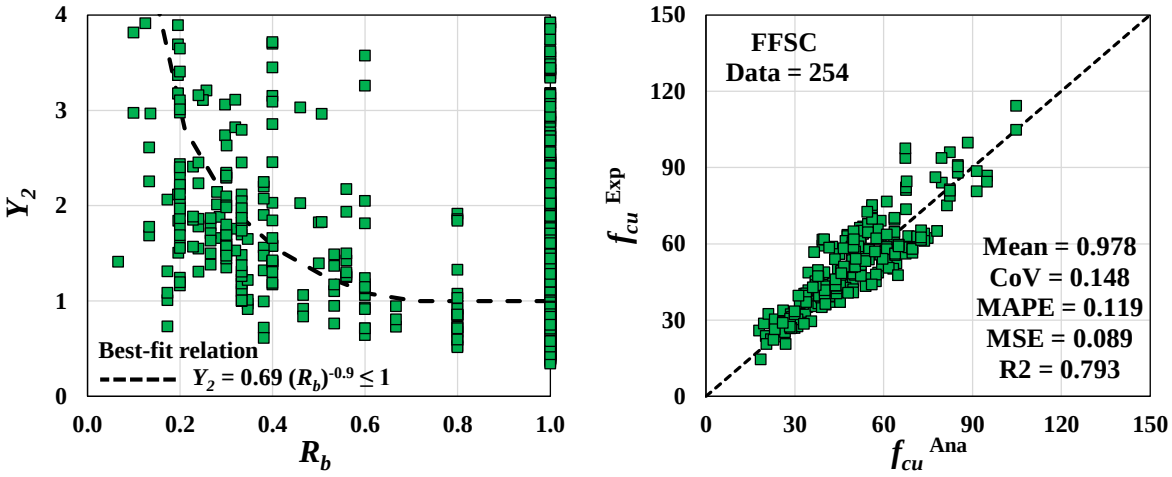

a) b)

Fig. 5. a) Relation of Y_2 versus R_b; b) Model performance of Eq. (14)

Fig. 6

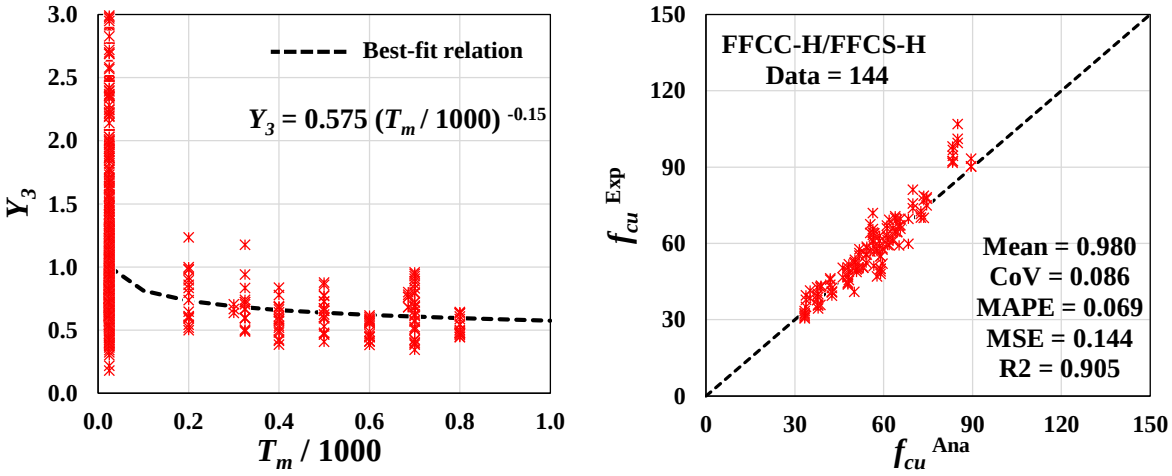

Fig. 6. a) Relation of Y_3 versus $T_m / 1000$; b) Model performance of Eq. (20)

Fig. 7

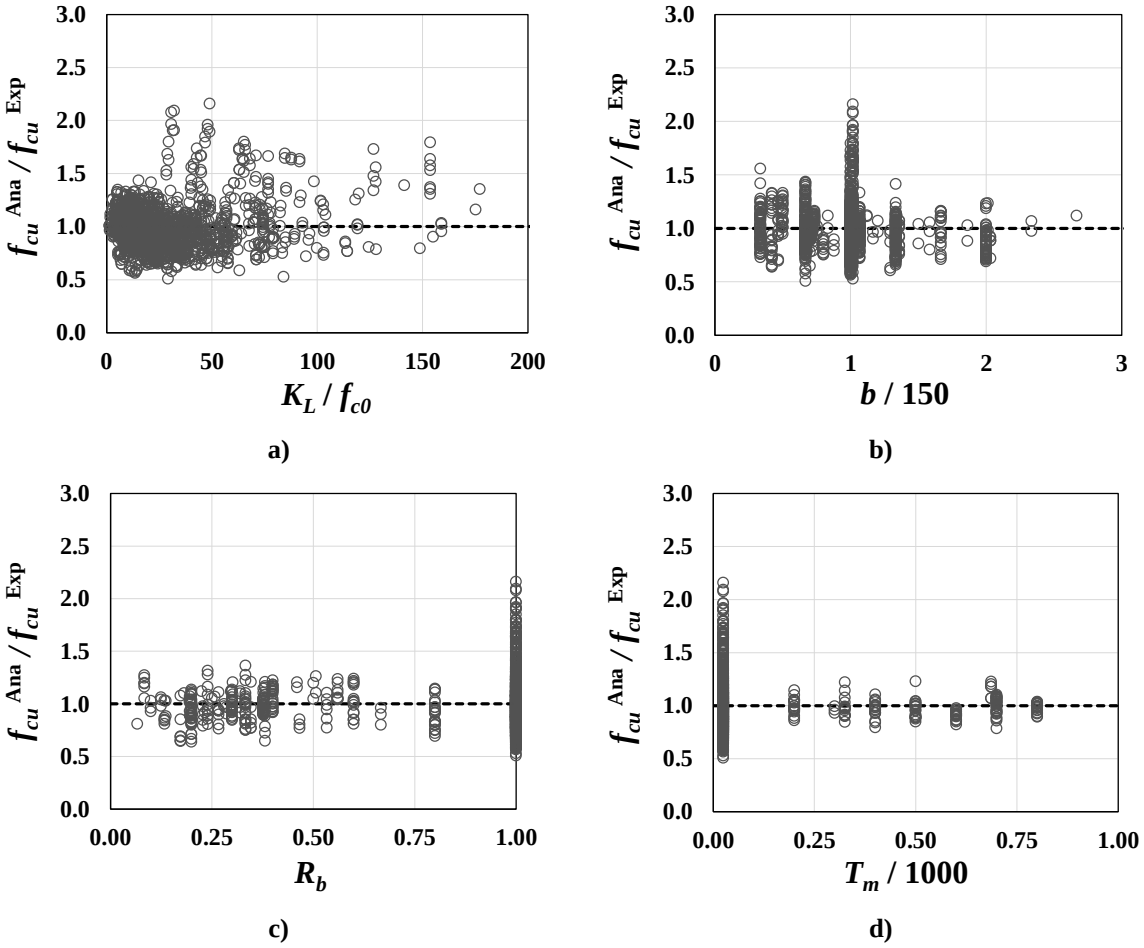

Fig. 7. Assessment of the predictive performance of Eq. (20)

Table 1

Table 1. Summary of the collected test database for FFCC, FFSC, FFCC-H and FFSC-H.

Confinement arrangement	Number of datasets		f_{c0} [a] range (MPa)	$\frac{f_{cu}}{f_{c0}}$ [b] range	L range (mm)	b range (mm)	E_f range (GPa)	ε_{fu} range	R_b [c]	T_m [d]
FFCC /FFSC FFCC-H /FFSC-H	1915	Min.	5.5	1.05	100	50	9.5	0.004	-	-
		Max.	204.0	13.8	1200	400	657	0.100	-	-
		MV	43.2	2.17	313	147	174	0.024	-	-
		CoV	0.723	0.562	0.370	0.297	0.589	0.782	-	-
FFCC	1517	Min.	6.6	1.05	100	50	9.5	0.004	1	25 [e]
		Max.	204.0	6.90	915	305	657	0.100	1	25
		MV	47.3	2.06	301	144	174	0.024	1	25
		CoV	0.700	0.414	0.352	0.295	0.614	0.801	0.000	0.000
FFSC	254	Min.	8.7	1.05	300	100	9.5	0.009	0.07	25
		Max.	77.2	4.32	1200	400	260	0.093	0.80	25
		MV	32.2	1.69	403	170	175	0.026	0.36	25
		CoV	0.402	0.336	0.392	0.303	0.532	0.792	0.527	0.000
FFCC-H/FFSC-H	144	Min.	5.5	1.39	200	100	105	0.017	0.38	200
		Max.	40.6	13.8	300	150	241	0.022	1	800
		MV	19.0	4.20	292	135	172	0.020	0.85	525
		CoV	0.585	0.624	0.095	0.158	0.374	0.101	0.315	0.369

a: For the heat-damaged specimens, the deteriorated compressive strength (f_{c0}^{T}) was used based on Eq. (1)

b: For the heat-damaged specimens, the confinement-induced improvements was calculated as f_{cu}/f_{c0}^{T} .

c: $R_b = 2r/b$ represents the corner radius ratio.

d: T_m represents the maximum exposure temperature based on the heating scheme (Fig. 1b).

e: For the case of the test specimens at ambient condition, T_m was assumed equal to 25 ℃ .

Table 2

Table 2. Existing axial strength models

ID	Model expression		Model parameters	
***fib* [21]**	$\frac{f_{cu}}{f_{c0}} = 1 + 3.3\frac{f_{l,rup}}{f_{c0}}$	for $\frac{f_{l,rup}}{f_{c0}} \geq 0.07$	$f_{l,rup} = 2k_h \frac{n_f t_f E_f}{b} \varepsilon_{h,rup}$	for $n_f \leq 3$
			$f_{l,rup} = 2k_h \frac{n_f^{0.85} t_f E_f}{b} \varepsilon_{h,rup}$	for $n_f \geq 4$
			$k_h = 1 - \frac{2(b-2r)^2}{3b^2}$	
	$\frac{f_{cu}}{f_{c0}} = 1$	for $\frac{f_{l,rup}}{f_{c0}} \leq 0.07$	$\varepsilon_{h,rup} = \eta_\varepsilon \varepsilon_{fu}$	
			$\eta_\varepsilon = 0.5\frac{r}{50}\left(2 - \frac{r}{50}\right)$	for $r \leq 60$ mm
			$\eta_\varepsilon = 0.5$	for $r > 60$ mm
CNR DT 200/2004 [17]	$\frac{f_{cu}}{f_{c0}} = 1 + 2.6\left(\frac{f_{l,rup}}{f_{c0}}\right)^{\frac{2}{3}}$	for $\frac{f_{l,rup}}{f_{c0}} \geq 0.05$	$f_{l,rup} = \frac{1}{2} k_h \rho_f E_f \varepsilon_{fd.rid}$	
			$\rho_f = \frac{4 n_f t_f}{b}$	
			$k_h = 1 - \frac{2(b-2r)^2}{3b^2}$	
	$\frac{f_{cu}}{f_{c0}} = 1$	for $\frac{f_{l,rup}}{f_{c0}} \leq 0.05$	$\varepsilon_{fd.rid} = \min\left\{\frac{\eta_a \varepsilon_{fu}}{\lambda_f}, 0.004\right\}$	
			η_a = 0.65, 0.75 and 0.85 for the fibre/resin type as Glass/Epoxy, Aramid/Epoxy and Carbon/Epoxy, respectively. λ_f = the partial factor recommended as 1.10.	
ACI 440.2R- 17 [20]	$\frac{f_{cu}}{f_{c0}} = 1 + 3.3\psi_f \frac{f_{l,rup}}{f_{c0}}$	for $\frac{f_{l,rup}}{f_{c0}} \geq 0.08$	$f_{l,rup} = 2\frac{n_f t_f E_f}{b} \varepsilon_{h,rup}$	for FFCC
			$f_{l,rup} = 2k_h \frac{n_f t_f E_f}{\sqrt{2}b} \varepsilon_{h,rup}$	for FFSC
	$\frac{f_{cu}}{f_{c0}} = 1$	for $\frac{f_{l,rup}}{f_{c0}} \leq 0.08$	$k_h = 1 - \frac{2(b-2r)^2}{3b^2}$	
			$\varepsilon_{h,rup} = 0.55\varepsilon_{fu}$	
Wei and Wu [18]	$\frac{f_{cu}}{f_{c0}} = 1 + 2.2\left(\frac{2r}{b}\right)^{0.72}\left(\frac{f_{l,u}}{f_{c0}}\right)^{0.94}$		$f_{l,u} = 2\frac{n_f t_f E_f}{b} \varepsilon_{fu}$	
Nistico and Monti [19]	$\frac{f_{cu}}{f_{c0}} = 1 + 2.2\left(\frac{2r}{b}\right)\frac{f_{l,u}}{f_{c0}}$		$f_{l,u} = 2\frac{n_f t_f E_f}{b} \varepsilon_{fu}$	

Table 3

Table 3. Statistical assessment of existing and proposed models for FFCC

ID	Test data	MV	CoV	MAPE	MSE	R^2
Proposed Model	1517	**0.989**	**0.218**	**0.160**	**0.298**	**0.842**
***fib* [21]**		0.903	0.226	0.183	0.336	0.812
ACI 440.2R- 17 [20]		0.948	0.273	0.188	0.366	0.806
CNR DT 200/2004 [17]		0.770	0.260	0.263	0.760	0.794
Wei and Wu [18]		1.089	0.276	0.196	0.426	0.807
Nistico and Monti [19]		1.045	0.298	0.187	0.428	0.798

Table 4

Table 4. Statistical assessment of existing and proposed models for FFSC

ID	Test data	MV	CoV	MAPE	MSE	R^2
Proposed Model	308	**0.978**	**0.148**	**0.119**	**0.089**	**0.793**
***fib* [21]**		0.888	0.173	0.154	0.170	0.778
ACI 440.2R- 17 [20]		0.900	0.206	0.165	0.178	0.668
CNR DT 200/2004 [17]		0.856	0.250	0.209	0.344	0.552
Wei and Wu [18]		0.987	0.159	0.121	0.096	0.792
Nistico and Monti [19]		0.881	0.161	0.151	0.178	0.790

Table 5

Table 5. Statistical assessment of existing and proposed models for FFCC-H/FFSC-H

ID	Test data	MV	CoV	MAPE	MSE	R^2
Proposed Model	144	**0.980**	**0.086**	**0.069**	**0.144**	**0.905**
***fib* [21]**		0.563	0.256	0.437	8.500	0.415
ACI 440.2R- 17 [20]		0.591	0.248	0.409	7.518	0.480
CNR DT 200/2004 [17]		0.487	0.346	0.513	11.73	0.576
Wei and Wu [18]		0.669	0.230	0.332	5.885	0.520
Nistico and Monti [19]		0.627	0.232	0.373	6.596	0.531

Table 6

Table 6. Statistical assessment of existing and proposed models for FFCC/FFSC/FFCC-H/FFSC-H

ID	Test data	MV	CoV	MAPE	MSE	R^2
Proposed Model	2031	**0.987**	**0.203**	**0.148**	**0.259**	**0.854**
***fib* [21]**		0.875	0.244	0.198	0.928	0.813
ACI 440.2R- 17 [20]		0.915	0.285	0.201	0.879	0.811
CNR DT 200/2004 [17]		0.760	0.285	0.274	1.529	0.789
Wei and Wu [18]		1.044	0.286	0.197	0.793	0.814
Nistico and Monti [19]		0.992	0.297	0.197	0.858	0.807